Advanced Review

State-to-state photodissociation dynamics of the water molecule

Xixi Hu,[1] Linsen Zhou[2] and Daiqian Xie[1]*

Photodissociation provides an ideal proving ground for an in-depth understanding of the microscopic mechanism and dynamics of bond breaking processes at a state-to-state level. After a brief outline of the requisite theory, we review the latest developments on the state-to-state photodissociation dynamics of the water molecule via the lowest two excited states, focusing on the absorption spectrum and product state distributions. A detailed discussion is given on the competition between different adiabatic and nonadiabatic pathways of the dissociation. Quantum mechanical studies of this prototypical system on accurate coupled potential energy surfaces not only offer an interpretation of the existing experimental results but also provide a clear and comprehensive dynamical picture of water photodissociation.

How to cite this article:
WIREs Comput Mol Sci 2018, 8:e1350. doi: 10.1002/wcms.1350

INTRODUCTION

Chemical reactions involve the breaking and forming of chemical bonds via complex rearrangement of both electrons and nuclei. In bimolecular reactions, a complete description of the collisional process requires the average over many partial waves.[1] As a result, many important dynamical features are often obscured in the measurable cross sections by averaging the initial orientation of the reactants and their impact parameters.[2,3] It is often more straightforward to study half collisional processes such as photodissociation, in which a stable molecule is brought from its ground electronic state to a dissociative excited state by absorption of one or more photons. The subsequent dissociation leads to molecular fragments, resembling the dissociation of the activated complex in a bimolecular reaction. The photoexcitation is instantaneous, allowing the accurate definition of time zero and thus enabling the real-time characterization of the dissociation process. Photodissociation also serves as models for a large class of chemical reactions initiated by light, such as vision,[4] atmospheric chemistry[5] and interstellar chemistry.[6] As a result, there has been a wide interest in studying the dynamics of photodissociation.[7–12]

Since photodissociation occurs on electronic excited state(s), the commonly used Born–Oppenheimer (B–O) approximation, which separates the electronic and nuclear motion, may break down completely.[13,14] Thus, it is essential to include all relevant electronic states and their couplings in characterizing photodissociation dynamics.[15]

Our knowledge about the dynamics of photodissociation has largely been acquired by the synergistic interplay between experimental and theoretical studies. Theoretically, quantum state resolved photodissociation dynamics provides us the remarkable detail of photodissociation reaction mechanism at a quantum state resolved level. However, accurate characterization of these processes is a very challenging endeavor. While the quantum mechanical formulation for simulating photodissociation dynamics has been established sometimes ago,[16] accurate coupled diabatic potential energy surfaces (PESs) were rarely available until recently, thanks to rapid advances in *ab initio* theory and fitting approaches that have made PESs and nonadiabatic couplings of polyatomic systems more reliable than before.[17–23] Despite

*Correspondence to: dqxie@nju.edu.cn

[1]Institute of Theoretical and Computational Chemistry, Key Laboratory of Mesoscopic Chemistry, School of Chemistry and Chemical Engineering, Nanjing University, Nanjing, China

[2]Department of Chemistry and Chemical Biology, University of New Mexico, Albuquerque, NM, USA

Conflict of interest: The authors have declared no conflicts of interest for this article.

extensive studies on photodissociation dynamics in polyatomic molecules,[10] quantitative agreements with experiments have just started to emerge for polyatomic systems dominated by nonadiabatic transitions.[15] One such example is the photodissociation of the water molecule.[24]

The photodissociation of water molecule is a central component in atmospheric chemistry and interstellar chemistry. It is considered as an ideal prototype for understanding reaction dynamics in polyatomic systems because of (1) its relative simplicity in the electronic structure and the small number of electrons that allows accurate *ab initio* determination of PESs, (2) its small number of degrees of freedom (DOFs) and the light mass of the hydrogen atoms that are amenable to full-dimensional quantum dynamical calculations, (3) the presence of several different kinds of nonadiabatic couplings, and (4) the abundant experimental data available to compare with.

In recent years, state-to-state photodissociation dynamics of H_2O have been carefully investigated at different excitation energies in many experimental and theoretical studies. The measured absorption cross sections of water in the 6.0–11.0 eV VUV region are shown in Figure 1. Four absorption bands (A, B, C, and D) exhibit distinct structures reflecting different dissociation mechanisms. Figure 1 also depicts one-dimensional cuts, along the dissociative OH bond, through the PESs of five singlet electronic states involved in the photodissociation: the bound ground state $\widetilde{X}^1A_1(^1A')$ and the first excited state $\widetilde{A}^1B_1(^1A'')$ correlating to the lower $OH(\widetilde{X}^2\Pi)$ + H asymptote, the second excited state $\widetilde{B}^1A_1(^1A')$ correlating adiabatically to $OH(\widetilde{A}^2\Sigma^+)$ + H asymptote, and higher bound Rydberg states $\widetilde{C}^1B_1(^1A'')$ and $\widetilde{D}^1A_1(^1A')$.

The absorption spectrum of the A band is broad and structureless, indicating a fast and direct bond breaking reaction on the single $\widetilde{A}^1A''$ PES. As a prototype of adiabatic dissociation process, this system has been extensively investigated by both experimental[26–34] and theoretical[35–39] studies and is considered as 'well-understood'.[10] The remaining questions include the OH population in its fine structures, for which only a simple Franck–Condon (FC) model exists.[30,40] Recently, we presented a full-dimensional wave packet study for OH Λ-doublet dynamics, which yielded a better agreement with the experimental data at 193 nm than those of FC model neglecting all dynamical effects of the exit-channel dynamics.[41] New insights concerning the dissociation dynamics was obtained.

The B band emerges from 140 nm and has a number of nearly equidistant diffuse peaks with a spacing of 810 cm^{-1} superimposed on a broad background. The structures have been interpreted as the resonances of bending and HO—H stretching motion.[42–47] The B band has also attracted extensive theoretical[42,43,45,46,48–60] and experimental[25,61–74] studies during the last few decades. It is well established that, in addition to the adiabatic pathway to the $OH(\widetilde{A}^2\Sigma^+)$ + H fragments, there are two nonadiabatic pathways leading to the $OH(\widetilde{X}^2\Pi)$ + H fragments: the $\widetilde{B} \rightarrow \widetilde{X}$ transition via the HOH and HHO conical intersections (CIs) and the $\widetilde{B} \rightarrow \widetilde{A}$ transition

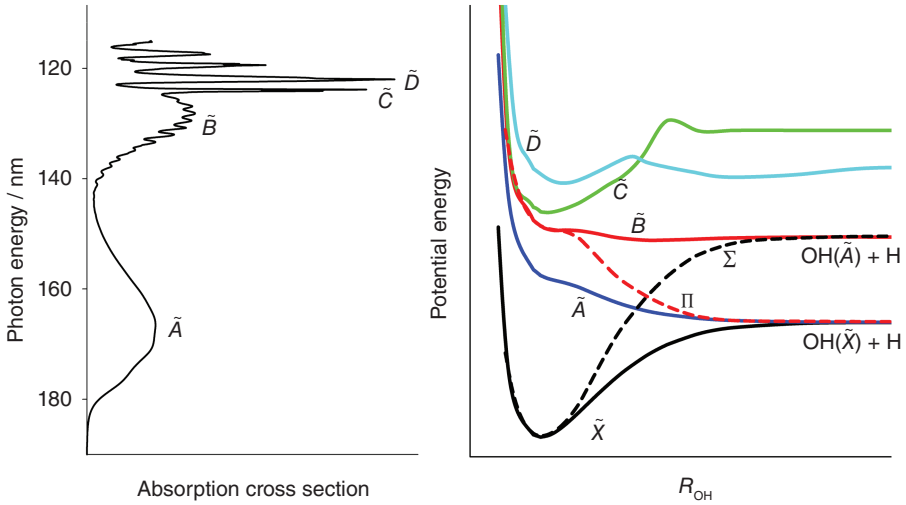

FIGURE 1 | The measured absorption spectra in room temperature for H_2O[25] and the one-dimensional schematic potential energy curves as a function of the dissociative OH bond with the other OH bond and the HOH angle kept at their equilibrium values of the ground state.

via the ro-vibronic or Renner–Teller (RT) coupling near linearity. These dissociation pathways are clearly shown in Figure 2, where the adiabatic PESs of relevant states are displayed. It has been shown that the nonadiabatic coupling is very strong and the ground OH($\tilde{X}^2\Pi$) + H channel is dominant for the whole energy range of the B band.[51,63]

Unlike the rapid (fs) dissociation of $\tilde{A}$ and $\tilde{B}$ states, the predissociation of the $\tilde{C}$ Rydberg state is much slower, in the order of a few picoseconds. The absorption spectrum around 124 nm shows sharp peaks and fully resolvable rotational structures can be identified.[62,76–79] The predissociation dynamics of the $\tilde{C}$ state depends strongly on the rotational quantum number and is an ideal model to study the rotational-state-specific dissociation dynamics.[24,80,81] The predissociation mechanism for this state has been studied extensively using multiphoton ionization and spontaneous fluorescence detection methods.[51,62,77–79,82,83] For example, Ashfold et al. obtained the fully resolved photo-fragment fluorescence spectrum and suggested two separate predissociation mechanisms, via one homogeneous, rotational state-independent, and one heterogeneous, rotational state-dependent pathway.[62,78,79] Yang and coworkers reported time-of-flight (TOF) spectra for the C band, which shows a dramatic variation in the product state distributions and its stereodynamics for different resonant levels.[81,84,85] The relative probabilities of these two pathways depend strongly on the rotational quantum number.[86,87] Dynamic calculations were performed on a new set of reduced-dimensional PESs for the $\tilde{X}$, $\tilde{A}$, $^1A_2$, $\tilde{B}$, and $\tilde{C}$ states and nonadiabatic transitions between those states.[88] The major dissociation route is via a two-step $\tilde{C} \rightarrow {}^1A_2 \rightarrow \tilde{A}$ indirect decay, while the direct $\tilde{C} \rightarrow \tilde{A}$ decay route is minor. Large discrepancies still exist between simulations and experiments, due to the lack of related full-dimensional PESs. Thus the details of the C band predissociation mechanism are still more or less obscure.

The absorption spectrum of the $\tilde{D}$ state is near 122 nm and shows no rotational structure, due to a strong interaction with the $\tilde{B}$ state at bent geometries.[46,89] The nonadiabatic coupling leads to a fast homogenous predissociation of $\tilde{D} \rightarrow \tilde{B}$ and shows purely electronic nature without isotope effect.[24] Steinkellner et al. concluded the lifetime of H_2O ($\tilde{D}$) on a time scale of around 50 fs using the femtosecond laser pump-probe technique.[90] Yuan et al. carried out a two-photon excitation dissociation dynamics study of the $\tilde{D}$ state using H atom Rydberg tagging time-of-flight (HRTOF) technique. The photodissociation action spectrum suggested the lifetime of this state about 13.5 fs. The ro-vibrational state distributions and angular distributions of the OH product are qualitatively similar to those of 121.6 nm H_2O photodissociation. This implies that photodissociation of the $\tilde{D}$ state proceeds via a fast electronically nonadiabatic conversion to the $\tilde{B}$ state and the main dynamical features eventually are determined by the topography of the $\tilde{B}$ PES.

In this review, we present the most recent developments in the *ab initio* calculations of the PESs and the quantum mechanical studies of the two lowest electronically excited states of H_2O. The total absorption cross sections, ro-vibrational state distributions and fine structure populations at several photon energies are compared with experiments, to present a clear dynamical picture of the fascinating nature of water photodissociation.

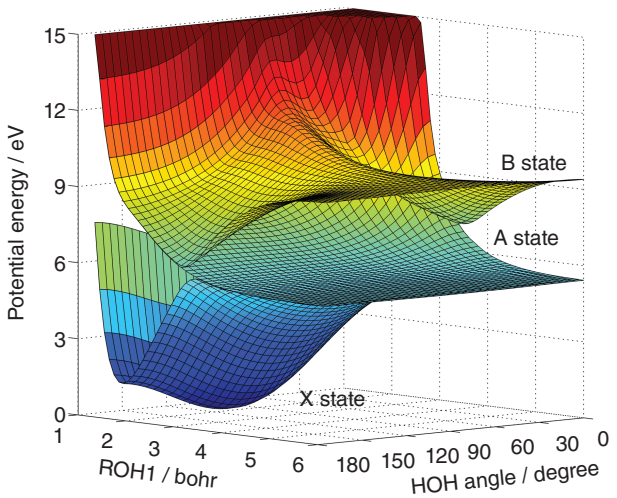

FIGURE 2 | The $\tilde{X}^1A'$, $\tilde{A}^1A''$, and $\tilde{B}^1A'$ adiabatic PESs for H_2O plotted in one O—H bond and H—O—H angle, with the other O—H bond fixed at the equilibrium distance. There are two CIs between the $\tilde{X}$ and $\tilde{B}$ states, one with HOH and another with HHO linear configurations. The three states form degenerate RT pairs at linearity. Adapted from Ref 75 with permission. Copyright (2013) American Chemical Society.

THEORETICAL TECHNIQUES

Potential Energy Surfaces

Accurate PESs are the pre-requisite of dynamics calculations.[17–23] For the nonadiabatic dynamics of H_2O ($\tilde{B}$), the breakdown of the B–O approximation leads to coupling between the electronic and nuclear

DOFs, especially near the electronic degeneracies. It is much more convenient in dynamical calculations to use the quasi-diabatic representation because it minimizes the derivative coupling.[13] Previously, there existed two global PESs (called DK and Leiden PESs) in the quasi-diabatic form that are suitable for studying the photodissociation dynamics of the B band. The DK PESs were based on *ab initio* points obtained using the internally contracted multi-reference configuration interaction (icMRCI) method.[91–93] Although widely used for bimolecular reaction dynamics studies, few details are available on how they were constructed.[94] The Leiden PESs, which was developed using a different MRCI method,[46,58] contains only 1560 points. To provide a more accurate understanding of the dissociation dynamics, we have calculated and fitted more than 13,000 *ab initio* points to a new set of global PESs for the lowest $\widetilde{X}$, $\widetilde{A}$, and $\widetilde{B}$ states of H_2O in a diabatic representation.[47,95] The electronic energies were computed using an icMRCI method with the augmented correlation-consistent polarized valence quadruple-ζ (aug-cc-pVQZ) basis set.[96] A large active space was used to describe the Rydberg characters of the excited states of H_2O and the Davidson correction was applied to approximately account for contributions of higher excitations and size consistency. All calculations including the transition moments were carried out using MOLPRO.[97] The adiabatic PESs of relevant states are displayed in Figure 2. Both the CIs and RT interactions are evident. The $\widetilde{A}^1A''$ state is repulsive and therefore the H—OH bond breaks immediately in its first band. The $\widetilde{B}$ state has two deep potential wells at the linear configurations, corresponding to HOH and HHO, due to the CIs between the $\widetilde{B}$ and $\widetilde{X}$ states. The locations of CIs and the PESs near CIs are the key factors not only for qualitative understanding but also for quantitative computations for photodissociation dynamics.

The diabatic states can be obtained from the adiabatic states using an orthogonal transformation[98,99] as follows:

$$\begin{pmatrix} |\Sigma\rangle \\ |\Pi\rangle \end{pmatrix} = \begin{pmatrix} \cos\alpha & \sin\alpha \\ -\sin\alpha & \cos\alpha \end{pmatrix} \begin{pmatrix} |1A'\rangle \\ |2A'\rangle \end{pmatrix} \quad (1)$$

The 'mixing angle' α, which is a function of the molecular geometry, can be obtained from the electronic angular momentum matrix elements as: $\alpha = \arcsin\sqrt{\left|\langle 1A''|\hat{L}_z|1A'\rangle\right|^2 + \left|\langle 1A''|\hat{L}_y|1A'\rangle\right|^2}$.[58] Then, the diabatic PESs and their coupling (V_Σ, V_Π, $V_{\Sigma\Pi}$) can be calculated from the adiabatic PESs ($V_{1A'}$, $V_{2A'}$): $V_\Sigma = V_{1A'}\cos^2\alpha + V_{2A'}\sin^2\alpha$, $V_\Pi = V_{1A'}\sin^2\alpha + V_{2A'}\cos^2\alpha$, and $V_{\Sigma\Pi} = \frac{1}{2}(V_{2A'} - V_{1A'})\sin 2\alpha$. The corresponding diabatic PESs and their coupling are presented in Figure 3, where one OH bond length is fixed at $1.8a_0$. The well in the coupling $V_{\Sigma\Pi}$ indicates that the nonadiabatic coupling is strongest there.

Quantum Dynamical Calculations

The photodissociation of water via the B band is depicted as follows:

$$\begin{aligned} H_2O\left(\widetilde{X},(v_1,v_2,v_3),J_{K_aK_c}\right) &\xrightarrow{h\nu} H_2O\left(\widetilde{B}\right) \\ &\xrightarrow{\text{adiabatic}} H + OH\left(A^2\Sigma^+,v,N,s_1,\Lambda\right) \\ &\xrightarrow{\text{CI/RT}} H_2O\left(\widetilde{X}/\widetilde{A}\right) \rightarrow H + OH\left(X^2\Pi,v,N,s_1,\Lambda\right) \end{aligned}$$

where (v_1, v_2, v_3) and $J_{K_aK_c}$ designate the initial rovibrational state of $H_2O(\widetilde{X})$, with the three vibrational quantum numbers representing the symmetric stretching, bending, and antisymmetric stretching modes, respectively. The $OH(\widetilde{X}/\widetilde{A})$ fragments are labeled by the vibrational (v), rotational-electronic (N), spin (s_1), and electronic (Λ) quantum numbers.

Firstly, we just consider the strong CIs coupling between $\widetilde{X}$ and $\widetilde{B}$ states. The two-state coupling model of Eq. (1) is employed and the spinless triatomic Hamiltonian in diabatic forms are given as:

$$\hat{H} = \hat{T}\mathbf{I} + \begin{bmatrix} V_\Sigma & V_{\Sigma\Pi} \\ V_{\Sigma\Pi} & V_\Pi \end{bmatrix} \quad (2)$$

where $\mathbf{I}$ is the two-dimensional identity matrix. $\hat{T}$ is the kinetic energy operator in the product H—OH(R) Jacobi coordinate.[100]

Since the diabatization procedure for RT coupling is also well established,[51,101,102] we combine this diabatization procedure with Eq. (1) to include both CIs and RT couplings in a three-state model. The orthogonal transformation between the two representations can be written as:

$$\begin{pmatrix} |\Sigma^{\lambda=0}\rangle \\ |\Pi^{\lambda=-1}\rangle \\ |\Pi^{\lambda=+1}\rangle \end{pmatrix} = \begin{pmatrix} \cos\alpha & \sin\alpha & 0 \\ -\frac{\sin\alpha}{\sqrt{2}} & \frac{\cos\alpha}{\sqrt{2}} & -\frac{i}{\sqrt{2}} \\ -\frac{\sin\alpha}{\sqrt{2}} & \frac{\cos\alpha}{\sqrt{2}} & \frac{i}{\sqrt{2}} \end{pmatrix} \begin{pmatrix} |1A'\rangle \\ |2A'\rangle \\ |1A''\rangle \end{pmatrix} \quad (3)$$

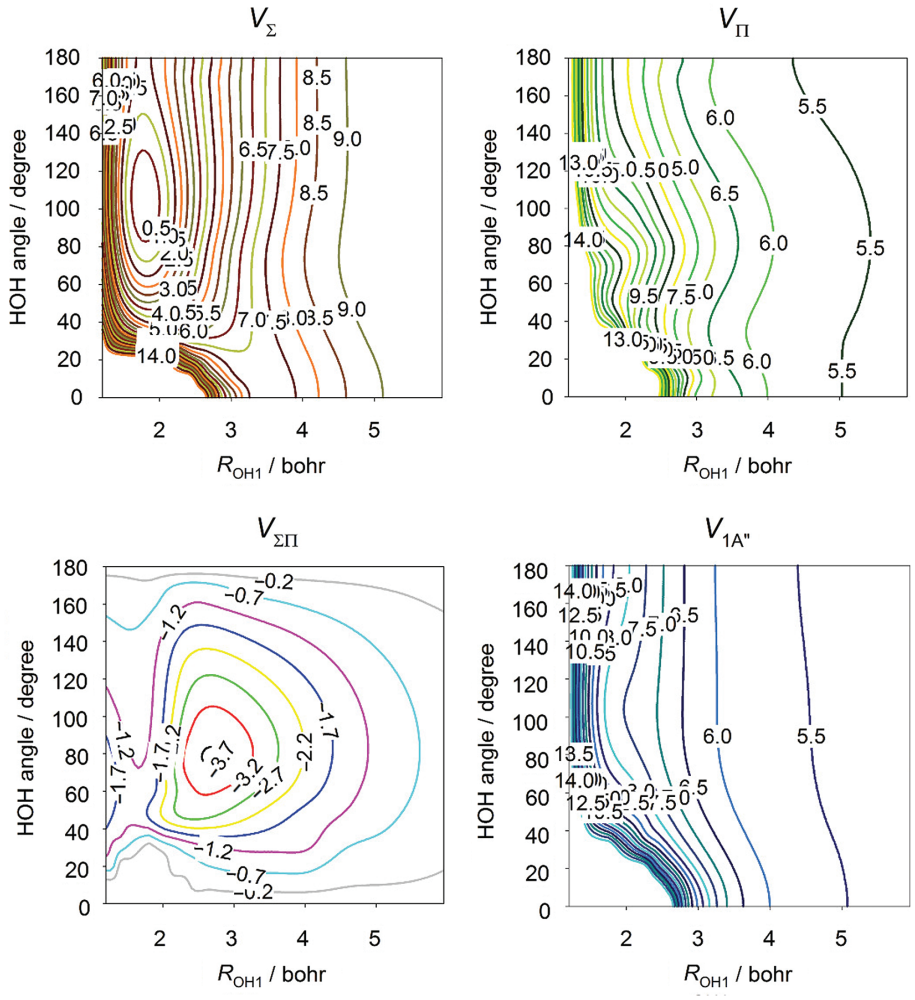

FIGURE 3 | Diabatic PESs for the diagonal (V_Σ, V_Π) and off-diagonal ($V_{\Sigma\Pi}$) terms, as well as the $1A''$ PES, as a function of R_{OH1} and the HOH angle, with the other OH bond fixed at $1.8a_0$. The contour intervals are 0.5 eV for all panels. Adapted from Ref 47 with permission.

where the diabatic states are labeled by the z component of electronic angular momentum with $\lambda = 0$, -1, and $+1$. This transformation defines a 3×3 diabatic potential energy matrix in the nuclear Hamiltonian. The nuclear kinetic energy operator in the Jacobi coordinates were given by Tennyson and Sutcliffe[103] and Petrongolo.[104] The corresponding parity-adapted rotational-electronic basis functions were defined in our previous work,[75,105] which are similar to those of van Harrevelt and van Hemert.[46,60]

We further consider the coupling of the nuclear and electronic DOFs in the OH fragment, which makes the description of the system quite complicated. For the OH fragment, the e and f levels in each Λ-doublet are associated with the parity $p = (-1)^{j\pm\frac{1}{2}}$.[106] Following Dixon, the fine structure of the fragment is described by the following basis:

$$\left|F_\tau; \Lambda s_1 j m_j p\right\rangle = A_\tau \left|N = j - \frac{1}{2}, \Lambda s_1 j m_j p\right\rangle + B_\tau \left|N' = j + \frac{1}{2}, \Lambda s_1 j m_j p\right\rangle \quad (4)$$

where j is the OH total angular momentum (excluding the nuclear spin) and m_j is its projection. $OH(\tilde{A}^2\Sigma^+)$ possesses two sublevels with $\tau = 1e, 2f$, and $OH(\tilde{X}^2\Pi)$ has four sublevels with $\tau = 1e, 1f, 2e, 2f$. $|N, \Lambda s_1 j m_j p|$ are the basis functions in Hund's case (b), and N is a good quantum number and expressed as the result of coupling between j and s_1.[107] The $OH(\tilde{A}^2\Sigma^+)$ product actually conforms to Hund's case (b), with $A_1 = B_2 = 1$ and $A_2 = B_1 = 0$. On the other hand, $OH(\tilde{X}^2\Pi)$ is intermediate in character between Hund's cases (a) and (b) for low values

of N, but reaches the Hund's case (b) limit at high values of N.

The propagation of the diabatic wave packets were performed in the Chebyshev order (ξ) domain via the three-term recursion relation with the Hamiltonian normalized to [−1, 1],[108–110]

$$\Psi_{\xi+1} = D\left(2\hat{H}_{\text{norm}}\Psi_{\xi} - D\Psi_{\xi-1}\right) \quad \text{for } \xi > 1 \qquad (5)$$

with $\Psi_1 = D\hat{H}_{\text{norm}}\Psi_0$. In the Condon model, the initial wave packet on the excited $\widetilde{B}$ state was represented as a product of ground state wave function and the transition dipole moment.[111] The damping factor D was applied at the grid edge to impose the outgoing boundary conditions. The analysis of wave packet was performed using the theories established by Balint-Kurti et al.[112–114] We just give a simple description here. The total cross section (absorption spectrum) can be simply obtained using a cosine Fourier transformation of the Chebyshev autocorrelation function.[110] The so-called photo-fragmentation T matrix elements contain all the information about the dissociation dynamics, in terms of which all the experimentally measurable cross sections may be expressed. T matrix elements can be evaluated by analysis of the asymptotically wave packet.[111,113,115–117] The wave packet is analyzed by passing an analysis line at a large value of the dissociation coordinate $R = R_{\infty}$, and the Chebyshev correlation functions C matrix are computed as an overlap between the two-dimensional wave packet cut and the asymptotic ro-vibrational eigen functions of the OH fragment, which can be converted to the energy domain quantities by a discrete Fourier transform.[110]

H_2O PHOTODISSOCIATION IN THE A BAND

The $\widetilde{A}^1A''$ PES is rather flat around the angles of the FC regions and purely repulsive along the dissociation O—H coordinate. In contrast to H_2S where an electronically nonadiabatic intersection exists between the lowest two $^1A''$ states,[99,118] the $\widetilde{A}^1A''$ state of H_2O is well separated from other electronic states, which renders the A band as a prototype of an electronically adiabatic dissociation process with a very low internal excitation of the OH($\widetilde{X}^2\Pi$) radical product. During the last three decades, several groups used the laser-induced fluorescence (LIF) method to detect the ro-vibrational states and Λ-doublet states of OH($\widetilde{X}^2\Pi$) product from the ground and excited vibrational states of H_2O at 157 and 196 nm,[27,30,32,34,40,119–122] the latter of which is the so-called vibrationally mediated photodissociation (VMP).[123]

On the theoretical side, Schinke and coworkers carried out extensive state-to-state quantum dynamics on an accurate PES[124] studied on A band.[29] Comparison of the calculated absorption spectrum with measured spectrum is almost perfect. The calculated cross sections and rotational distributions were in good agreement with those of LIF experiment, but disagreement existed obviously in the vibrational distribution at 157 nm.[29] In 1999, Hwang et al. employed the HRTOF to quantitatively measure vibrational distributions at 157 nm, which suggested inaccuracy in LIF measurements.[125] According to the HRTOF results, van Harrevelt and van Hemert calculated vibrational distributions using the Leiden PESs at 157 nm.[126] It was found that the calculated OH($\widetilde{X}$) or OD($\widetilde{X}$) vibrational distributions were in better agreement with the kinetic energy release measurements of the H or D atoms produced in the 157.6 nm photodissociation of water and its isotopomers.[127] Balint-Kurti developed a simple FC model to account for the OH fine structure populations.[39] While such a model had been reasonably successful in predicting many qualitative features of the experiments,[27,119] it is not entirely satisfactory due to the neglect of the dissociation dynamics.[30,40] More recently, we presented a full-dimensional wave packet study for OH Λ-doublet dynamics and reported the OH fine structure populations in the A band, using the new PES developed by us.[47] The results are in better agreement with those experimental data at 193 nm than those of the FC model, presumably due to neglect of the exit-channel dynamics in FC model.[41] The calculated absorption spectrum on this PES is broad and structureless, agrees well with the experimental spectrum with slightly red shifted.[25,128] This small discrepancy might owe to the underestimation of the vertical excitation energy in the *ab initio* calculations. In addition, the experimental spectra were measured at room temperature where hot bands might contribute, while the theoretical one is calculated from the ground ro-vibrational state of $H_2O(\widetilde{X})$.

The calculated OH($\widetilde{X}^2\Pi$) product vibrational state distribution on the new PES, with a slight population inversion at $v = 1$ state, is in good agreement with the experimental result of Hwang et al.,[125] as shown in Figure 4. For the spin–orbit population

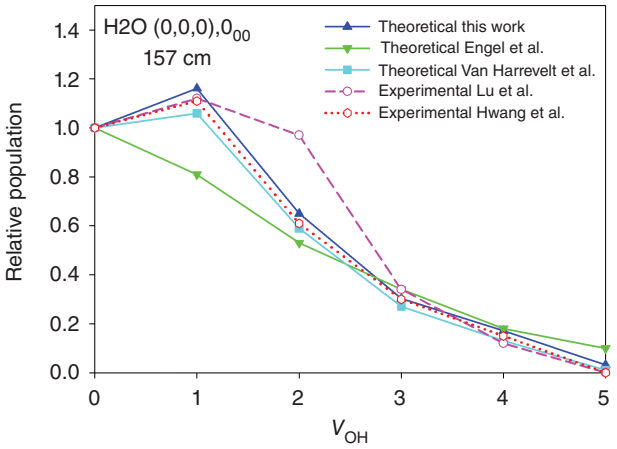

FIGURE 4 | The relative vibrational state distributions of the OH($\widetilde{X}$) product obtained from several theoretical and experimental studies. Adapted from Ref 41 with permission.

ratios of OH in its low-lying vibrational channels upon 157 nm photodissociation, significant departure from the statistical limit was found by Lu et al. who fit the translational distribution of the H fragment using the Rydberg tagging technique.[129] As shown in Figure 5, our calculated spin–orbit population ratios are different from the nonstatistical distributions reported by Lu et al.,[129] but agree well with the earlier data from Andresen et al.[32] and Plusquellic et al.[120] based on spectroscopy. The populations of the two spin–orbit manifolds are close to the statistical limit in most cases, but the Λ-doublet is dominated by the A'' component, due to the fast in-plane dissociation of $H_2O(\widetilde{A}^1A'')$. Interestingly, the similar distributions up to five quanta of OH from the photodissociation of the 0_{00} state of H_2O (0, 0, 1) suggesting that the influence of parent vibrational excitation is relatively minor for the OH rotational state distribution, consistent with the weak stretch-bend coupling in this system.[29,30] In general, our dynamical calculations were in better agreement with the experimental data than the previous theory. However, there are still some minor differences between theoretical and experimental results, which might be due to either approximations in the theoretical model, such as the neglect of spin–orbit coupling in the interaction region and the nearby triplet states, or uncertainties in experiments.

H_2O PHOTODISSOCIATION IN THE B BAND

The photodissociation dynamics in the B band involves three lowest nonadiabatic coupled electronic states and the related mechanisms are more complicated. In 1986, Ashfold et al. utilized the photofragment recoil spectroscopy technique to analysis the H atom TOF spectra at photon energies around 10 eV.[63] It revealed that the OH($\widetilde{X}$) fragments were formed predominantly in the ground vibrational level with a highly excited and inverted rotational state population distribution. Schinke and coworkers systematically calculated the absorption spectra and interpreted the diffuse progression of bands as the so-called unstable periodic orbits.[42,43,45] In 1994, Dixon and coworkers theoretically and experimentally studied the rotational distributions at 121.6 nm and described the RT interaction between $\widetilde{B}$ and $\widetilde{A}$ states scaling with the amount of *a*-axis rotational excitation in parent molecule.[64] Yang and coworkers[65,68] observed striking even–odd population oscillations in the rotational state distribution of the OH ($\widetilde{X}$, v = 0) product at 121.6 nm. Their quantum wave packet calculations, obtained with a reduced-dimensional approximation based on the Leiden PESs, attributed such oscillations to dynamical interference arising through the existence of the two CIs between the $\widetilde{B}$ and $\widetilde{X}$ states.[65,68] In 2000, van Harrevelt and van Hemert used a three-state model to study the absorption spectra, ro-vibrational distributions of OH fragment, and electronic branching ratios, which agreed qualitatively with the available experimental results except some differences in the absorption spectra. In 2011, Yang and coworkers reported state-resolved differential cross sections (DCSs) and studied the effects of different unstable resonances on the ground and excited product channels around 130 nm.[74] Although there has been no spectroscopic measurement of OH fine-structure distributions for the B band photodissociation, evidence has been presented for a nonuniform distribution of its Λ-doublet states.[65] Dixon presented a dynamical theory on the Λ-doublet population of OH for the B band. Based on the reduced-dimensional model and inaccurate PESs, several theoretical studies have explored the photodissociation dynamics with a fine-structure resolution.[64,65]

Based on the more accurate coupled diabatic PESs developed by Jiang et al.,[47] full-dimensional quantum mechanical studies of the state-to-state dissociation dynamics yielded excellent results in agreement with many latest experimental results. In our earlier work,[47,95] since the RT coupling was demonstrated to play a relatively minor role in the photodissociation, the two-state coupling model including only the $\widetilde{B}$ and $\widetilde{X}$ states coupled by the CIs was employed. Later, we extended the theoretical model

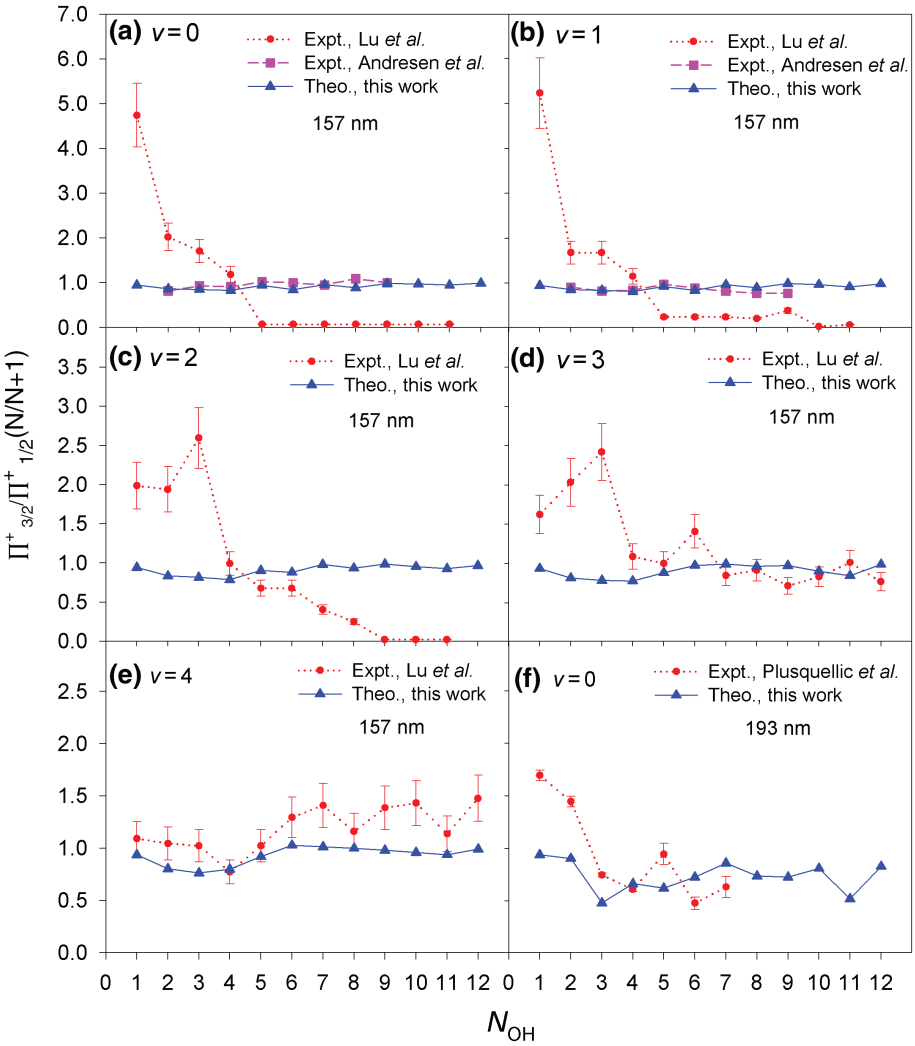

FIGURE 5 | Population ratios of the two spin–orbit components ($\Pi^+_{3/2}$ and $\Pi^+_{1/2}$) of the OH product in its low-lying vibrational channels upon the photodissociation of $H_2O(\tilde{X}, (0, 0, 0))$ obtained from several theoretical and experimental studies. Adapted from Ref 41 with permission.

to include all three ($\tilde{B}$, $\tilde{A}$, and $\tilde{X}$) electronic states and focused on the competing nonadiabatic pathways leading to the $OH(\tilde{X}^2\Pi)$ + H fragments and their impact on state-resolved attributes.[75] For the total cross section shown in Figure 6, the oscillating peaks have been attributed to metastable resonances in the well created by the CI near the HOH linearity.[43,46,130] The theoretical models with and without the RT coupling yielded similar results, which are in better agreement with experimental data than previous theoretical studies.[43,46,130]

As shown in Figure 2, the $\tilde{B}$ state has deep potential wells near the two collinear CIs and is steeply repulsive in the FC region, so that the photoexcited molecule experiences a strong torque along the dissociation path. Nonadiabatic transitions to lower electronic states are mostly direct and fast, leading to the dominance of the $OH(\tilde{X}^2\Pi)$ fragment with little vibrational excitation and a strong rotational excitation. As shown in Figure 7, the rotational state distribution of $OH(\tilde{X}, v = 0)$ is highly inverted with a peak near the highest allowed rotational state, indicating that most of the energy release in the dissociation is deposited into the rotational DOF. While the rotational state distribution of the OH ($\tilde{A}$, $v = 0$) fragment is much cooler that the ground state, due to the smaller anisotropy of the excited state PES. Although similar to our earlier results obtained without the RT coupling, the calculated results with the RT coupling are in better agreement with the experimental distributions. Both nonadiabatic pathways lead to rotational excited

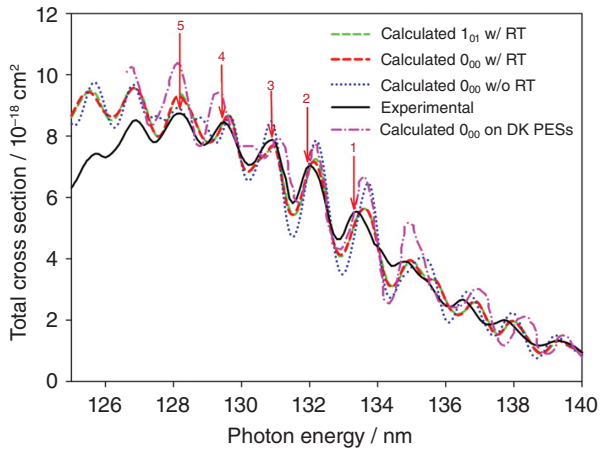

FIGURE 6 | Calculated total photodissociation cross sections from the 0_{00} (red-dashed line) and 1_{01} (green-dashed line) states, compared with the results of 0_{00} state without the RT coupling (blue-dotted line), the calculated results based on DK PESs (pink dash-dotted line), and the experimental spectrum (black solid line). Adapted from Ref 75 with permission. Copyright (2013) American Chemical Society.

OH($\widetilde{X}$) fragments, but the RT pathway results in much less rotational excitation. This is due to the fact that the torque force along this pathway is much gentler than that associated with the CI. In addition, the nonadiabatic pathway via the CI dominates in all wavelengths, consistent with the earlier theoretical results of Dixon.[56] The DCSs of both products show strong parallel characteristic for the $\widetilde{B} \rightarrow \widetilde{X}$ transition as in Figure 8. This is because the fast dissociation to OH($\widetilde{X}^2\Pi$) gives rise to product angular distributions that are parallel to the laser polarization for this parallel transition. Agreeing with previous reduced-dimensional models,[68] the oscillations in the rotational state distribution are assigned to a quantum interference between waves come from the HOH and HHO CIs in the $\widetilde{B} \rightarrow \widetilde{X}$ nonadiabatic pathways. This interference is also verified by the calculated rotational state-specific anisotropy parameter β which also show a clear even–odd oscillation. The rotational state distributions of OH($\widetilde{A}$) product change dramatically with photon wavelength, due to different long-lived resonances in HOH and HHO potential wells. However, the agreement between the calculated results and experimental one is less satisfactory. The discrepancies mainly stem from the inaccuracy of the adiabatic PES. To improve the PES, the electronic structure calculations should include more higher excited states, such as the D state, and employ a Dunning's basis set with extra *d* and *f* diffusion functions for oxygen to describe the substantial Rydberg nature.

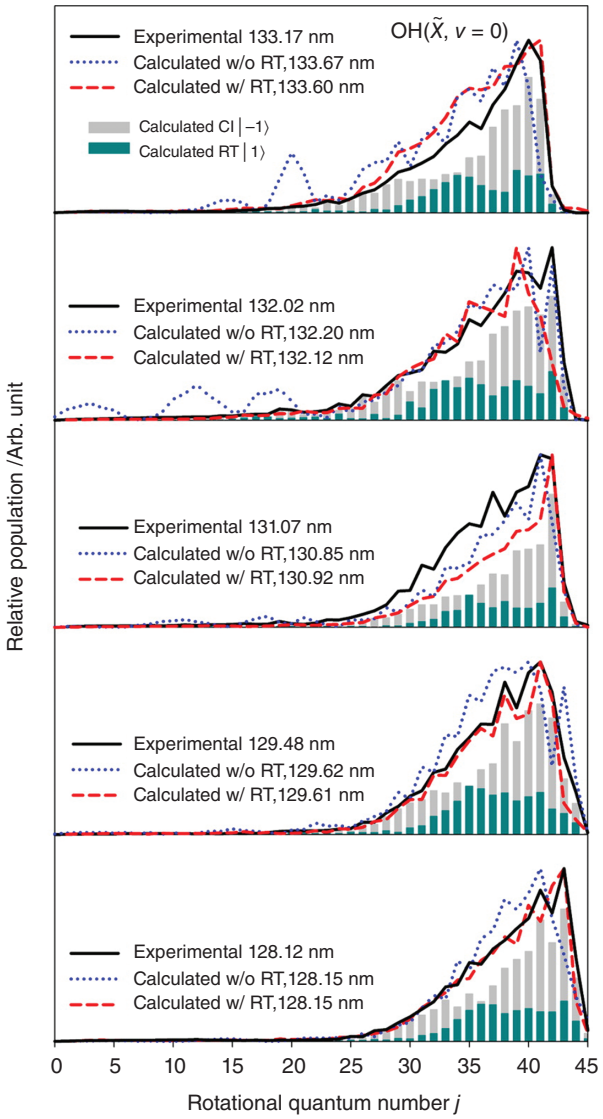

FIGURE 7 | Rotational state distributions of the OH ($\widetilde{X}$, v = 0) fragment at the five peak energies. The populations from the two nonadiabatic pathways via the CI and via the RT coupling are given in gray and dark cyan bars. Theoretical distributions with RT coupling (red-dashed lines), without RT coupling (blue-dotted lines) and the experimental distributions (black solid lines) are included. Adapted from Ref 75 with permission. Copyright (2013) American Chemical Society.

ISOTOPE EFFECTS

Isotope effects in photodissociation are also an interesting topic. The substitution of hydrogen by deuterium has no impact on the electronic structure, but often changes dynamical processes significantly, particularly where nonadiabatic forces such as CIs are involved.[70,86–88,131] The dissociation mechanism for D_2O is quite similar to that of H_2O, but there are

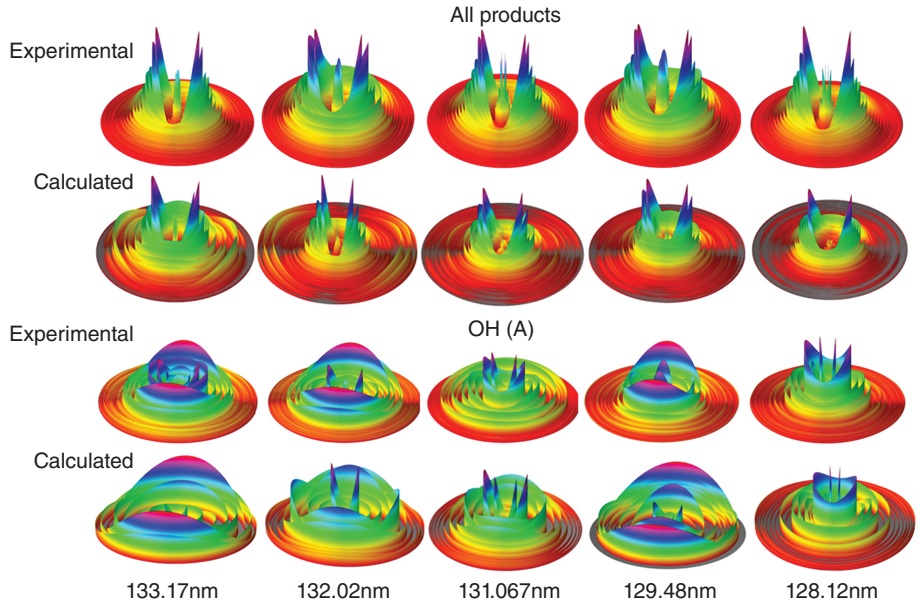

FIGURE 8 | Comparison of experimental and calculated differential cross sections at the five peak energies. Adapted from Ref 95 with permission.

some important quantitative differences. For the A band of D_2O photodissociation, seven vibrational features have been observed at 157.6 nm. Because of the smaller OD rotational constant, the rotational structures are not as well resolved as in the H_2O case. Even though more vibrational states of the OD product are populated than the OH product, the vibrational energy deposited into the OD product is quite similar to the OH product. For the B band of D_2O photodissociation, the dissociation products are mainly populated into nonadiabatic $OD(\widetilde{X})$ + D channel. The nonadiabatic channel via the DOD CI is direct and fast, which produces hot rotational and cold vibrational $OD(\widetilde{X})$ product, while the adiabatic channel is dominated by long-lived resonances which depends sensitively on the PESs. The experimental and calculated product distributions and angular distributions for the $OD(\widetilde{A})$ fragments change dramatically with the photolysis energy, due to a combination of fast direct dissociation and slow resonance decay.[132] Theoretically, state-to-state photodissociation dynamics of vibrationally excited D_2O in B band have been explored.[133] The calculated absorption spectra, product state distributions, and branching ratios from different initial vibrational states show different dynamic features, due to the different forms of the vibrational wave functions. The angular anisotropy parameters β of the OD ($\widetilde{X}$, $v = 0$) product exhibit fewer oscillations than those for H_2O and the branching ratio $OD(\widetilde{X})/OD(\widetilde{A})$ of 3.9 is significantly lower than that of 5.1 for $OH(\widetilde{X})/OH(\widetilde{A})$ at 121.6 nm.[68] The D_2O absorption spectrum has the amplitudes of the resonances almost a factor of 2 smaller than those for H_2O.[73] The OD ($\widetilde{X}$, $v = 0$) product has higher levels of rotational angular momentum than the corresponding OH ($\widetilde{X}$, $v = 0$) product.[134]

The substitution of one hydrogen in H_2O by a deuterium results in symmetry breaking and opens two distinct D + OH and H + OD dissociation channels, showing different dynamics behaviors. For the A band, the VMP with OD or OH bond preexcitation accesses different regions of the PES likely leading to mode or isotopic selectivity,[8,135] which has been a hot topic in photodissociation dynamics studies.[123] The theoretical[136–140] and experimental[29,40,120,141–145] studies of HOD in the A band have verified that OH/OD branching ratio can be 'steered' by choosing the appropriate initial vibrational state and photon wavelength. For the B band, the outcome of dissociation of HOD is quantitatively not the average of those for H_2O and D_2O.[69,70] For the photodissociation of HOD at 121.6 nm, OH ($\widetilde{X}$, $v = 0$) product shows 'super excited' rotational states above its dissociation limit and OD ($\widetilde{A}$, $v = 0$) product has an unusually strong population for a single rotational state labeled 'single rotational product propensity', which was not found in H_2O/D_2O photodissociation and HOD with D detection at 121.6 nm.[59,70,131] Recently, the

dynamics of the OD + H and OH + D channels of the HOD dissociation around 128 nm was investigated experimentally.[146] It should be noted that in the C band an interesting discovery is the symmetry-induced population oscillation that the high vibrational states of OH($\widetilde{X}$) and OD($\widetilde{X}$) exhibit a population alternation with the rotational quantum number. What is more, a clear alternation in vibrational population with odd v favored over even v was also observed experimentally for the OH($\widetilde{X}$) product in the C band.[88] Recently, the state-to-state quantum dynamics of the B band VMP was investigated using the three-state coupling model.[147] The product state distributions of OH($\widetilde{X}$) from four vibrational states are highly hot rotational excitation and very cold vibrational excitation, similar to the photodissociation of H_2O. For the OD($\widetilde{X}$) + H channel, the vibrational state distributions from HOD (0, 1, 0) are inverted with a peak at v = 1 at some photoenergies. The rotational state distributions of OD($\widetilde{X}$) from four vibrational states show two different behaviors. One has a single broad peak, while the other has a bimodal structure with a very pronounced peak near the highest allowed rotational state and a broad peak at lower rotational states. The calculated branching ratios OH($\widetilde{A}$)/OH($\widetilde{X}$) lower than 1.0 indicate that the nonadiabatic pathway dominates for the D dissociation throughout the whole energy range, while for OD + H channel, the nonadiabatic pathway only dominates at low energy.

CONCLUSIONS

The photodissociation dynamics of the water molecule has served as a prototype for understanding bond breaking dynamics in molecules. In this review, we summarized the latest theoretical studies using full-dimensional quantum mechanical models with accurate PESs. The inclusion of all relevant electronic states and their couplings results in an improved agreement with the latest experimental data and sheds valuable insights into the mechanism of water photodissociation. The detailed theoretical characterization of the photodissociation of H_2O reviewed here suggests that exquisite experimental measurements, such as absorption spectrum and product state distributions can now be quantitatively predicted with quantum dynamical calculations for small molecules. Such achievements can only be accomplished with highly accurate global PESs based on high level *ab initio* calculations and exact full-dimensional quantum dynamics. These theoretical studies can not only serve as benchmarks for more approximate models but also offer valuable insight into the reaction dynamic and nonadiabatic transitions for many important chemical processes. However, there are still some challenges in this field. For example, the photodissociation mechanism of water via the $\widetilde{C}$ state is still not well-understood. It is generally acknowledged that this process is a nonadiabatic dissociation process involving four states, which has two distinctive predissociation pathways. One is $\widetilde{C} \rightarrow \widetilde{B}$ pathway proceeding via Coriolis-type coupling. The other is $\widetilde{C} \rightarrow \widetilde{A}$ pathway through vibronic coupling.[24] Since there is a large energy gap between the FC region of $\widetilde{C}$ and $\widetilde{A}$ states, the $\widetilde{C} \rightarrow \widetilde{A}$ decay via a direct transition or an indirect process through the coupling between intermediate states is still disputed. The highly accurate diabatic PESs for relevant excited states and state-to-state photodissociation dynamics calculations will shed new light on the detailed microscopic mechanism of the photodissociation of water on higher bands.

ACKNOWLEDGMENTS

This work was supported by National Natural Science Foundation of China (Grant No. 91641104 to XH, 21590802 and 21733006 to DX), the Chinese Ministry of Science and Technology (Grant Nos. 2013CB834601 and 2017YFA0206501 to DX). LZ thanks support from the China Scholarship Council (Grant No. 201604890009). We sincerely thank Prof. Hua Guo and Prof. Bin Jiang for collaboration and many useful discussions.

REFERENCES

1. Levine RD. *Molecular Reaction Dynamics*. Cambridge: Cambridge University Press; 2005.
2. Zhang DH, Guo H. Recent advances in quantum dynamics of bimolecular reactions. *Annu Rev Phys Chem* 2016, 67:135–158.
3. Ren ZF, Sun ZG, Zhang DH, Yang XM. A review of dynamical resonances in A + BC chemical reactions. *Rep Prog Phys* 2017, 80:026401.
4. Kukura P, McCamant DW, Yoon S, Wandschneider DB, Mathies RA. Structural

observation of the primary isomerization in vision with femtosecond-stimulated raman. *Science* 2005, 310:1006–1009.

5. Finlayson-Pitts BJ, Pitts JN Jr. *Atmospheric Chemistry*. New York: John Wiley & Sons; 1986.
6. Tielens AGGM. *The Physics and Chemistry of the Interstellar Medium*. Cambridge: Cambridge University Press; 2005.
7. Ashfold MNR, Baggott JE. *Molecular Photodissociation Dynamics*. London: The Royal Society of Chemistry; 1987.
8. Crim FF. Vibrationally mediated photodissociation: exploring excited-state surfaces and controlling decomposition pathways. *Annu Rev Phys Chem* 1993, 44:397–428.
9. Butler LJ, Neumark DM. Photodissociation dynamics. *J Phys Chem* 1996, 100:12801–12816.
10. Schinke R. *Photodissociation Dynamics*. Cambridge: Cambridge University Press; 1993.
11. SR Y, Yuan DF, Chen WT, Xie T, Wang SW, Yang XM, Wang XA. High-resolution experimental study on photodissocaition of N_2O. *Chin J Chem Phys* 2016, 29:135–139.
12. Zhao ZQ, Liu S, Zhang DH. Differential cross sections for the H + D_2O → HD + OD reaction: a full dimensional state-to-state quantum dynamics study. *Chin J Chem Phys* 2017, 30:16–24.
13. Yarkony DR. Nonadiabatic quantum chemistry: past, present, and future. *Chem Rev* 2012, 112:481–498.
14. Klessinger M, Michl J. *Excited States and Photochemistry of Organic Molecules*. New York: VCH; 1995.
15. Guo H, Yarkony DR. Accurate nonadiabatic dynamics. *Phys Chem Chem Phys* 2016, 18:26335–26352.
16. Balint-Kurti GG, Shapiro M. Quantum theory of molecular photodissociation. In: *Photodissociation and Photoionization*. New York: John Wiley & Sons; 1985, 403–450.
17. Zhu X, Yarkony DR. On the representation of coupled adiabatic potential energy surfaces using quasi-diabatic Hamiltonians: description of accidental seams of conical intersection. *Mol Phys* 2010, 108:2611–2619.
18. Jiang B, Li J, Guo H. Potential energy surfaces from high fidelity fitting of *ab initio* points: the permutation invariant polynomial-neural network approach. *Int Rev Phys Chem* 2016, 35:479–506.
19. Majumder M, Ndengue SA, Dawes R. Automated construction of potential energy surfaces. *Mol Phys* 2016, 114:1–18.
20. Manzhos S, Dawes R, Carrington T. Neural network-based approaches for building high dimensional and quantum dynamics-friendly potential energy surfaces. *Int J Quantum Chem* 2015, 115:1012–1020.
21. Dawes R, Ndengue SA. Single- and multi-reference electronic structure calculations for constructing potential energy surfaces. *Int Rev Phys Chem* 2016, 35:441–478.
22. Wittenbrink N, Venghaus F, Williams D, Eisfeld W. A new approach for the development of diabatic potential energy surfaces: hybrid block-diagonalization and diabatization by ansatz. *J Chem Phys* 2016, 145:184108.
23. Zhu XL, Yarkony DR. Constructing diabatic representations using adiabatic and approximate diabatic data—coping with diabolical singularities. *J Chem Phys* 2016, 144:044104.
24. Yuan K, Dixon RN, Yang X. Photochemistry of the water molecule: adiabatic versus nonadiabatic dynamics. *Acc Chem Res* 2011, 44:369–378.
25. Mota R, Parafita R, Giuliani A, Hubin-Franskin MJ, Lourenco JMC, Garcia G, Hoffmann SV, Mason NJ, Ribeiro PA, Raposo M, et al. Water VUV electronic state spectroscopy by synchrotron radiation. *Chem Phys Lett* 2005, 416:152–159.
26. Andresen P, Beushausen V, Hausler D, Lulf HW, Rothe EW. Strong propensity rules in the photodissociation of a single rotational quantum state of vibrationally excited H_2O. *J Chem Phys* 1985, 83:1429–1430.
27. Hausler D, Andresen P, Schinke R. State to state photodissociation of H_2O in the first absorption band. *J Chem Phys* 1987, 87:3949–3965.
28. Schinke R, Vanderwal RL, Scott JL, Crim FF. The effect of bending vibrations on product rotations in the fully state-resolved photodissociation of the *A* state of water. *J Chem Phys* 1991, 94:283–288.
29. Engel V, Staemmler V, Vanderwal RL, Crim FF, Sension RJ, Hudson B, Andresen P, Hennig S, Weide K, Schinke R. Photodissociation of water in the first absorption band: a prototype for dissociation on a repulsive potential energy surface. *J Phys Chem* 1992, 96:3201–3213.
30. Brouard M, Langford SR, Manolopoulos DE. New trends in the state-to-state photodissociation dynamics of $H_2O(\tilde{A})$. *J Chem Phys* 1994, 101:7458–7467.
31. Grunewald AU, Gericke K-H, Comes FJ. Photodissociation of room temperature and jet-cooled water at 193 nm. *Chem Phys Lett* 1987, 133:501–506.
32. Andresen P, Ondrey GS, Titze B, Rothe EW. Nuclear and electron dynamics in the photodissociation of water. *J Chem Phys* 1984, 80:2548–2569.
33. Mikulecky K, Gericke KH, Comes FJ. Decay dynamics of $H_2O(^1B_1)$: full characterization of OH product state distribution. *Chem Phys Lett* 1991, 182:290–296.
34. Schinke R, Engle V, Andresen P, Hausler D, Balint-Kurti GG. Photodissociation of single H_2O quantum states in the first absorption band: complete

characterization of OH rotational and Λ-doublet state distributions. *Phys Rev Lett* 1985, 55:1180–1183.

35. Schinke R, Engel V, Staemmler V. *Ab initio* study of the photodissociation of water: OH state distributions and comparison with experiment. *Chem Phys Lett* 1985, 116:165–168.
36. Hennig S, Engel V, Schinke R, Staemmler V. Emission spectroscopy of photodissociating water molecules: a time-independent *ab initio* study. *Chem Phys Lett* 1988, 149:455–462.
37. Kühl K, Schinke R. Time-dependent rotational state distributions in direct photodissociation. *Chem Phys Lett* 1989, 158:81–86.
38. Zhang JZ, Imre DG. Spectroscopy and photodissociation dynamics of H_2O: time-dependent view. *J Chem Phys* 1989, 90:1666–1676.
39. Balint-Kurti GG. Dynamics of OH Λ-doublet production through photodissociation of water in its first absorption band. I. Formal theory. *J Chem Phys* 1986, 84:4443–4454.
40. Brouard M, Langford SR. The state-to-state photodissociation dynamics of HOD($\tilde{A}$). *J Chem Phys* 1997, 106:6354–6364.
41. Zhou LS, Xie DQ, Sun ZG, Guo H. Product fine-structure resolved photodissociation dynamics: the *A* band of H_2O. *J Chem Phys* 2014, 140:024310.
42. Weide K, Schinke R. Photodissociation dynamics of water in the second absorption band. II. *Ab initio* calculation of the absorption spectra for H_2O and D_2O and dynamical interpretation of "diffuse vibrational" structures. *J Chem Phys* 1989, 90:7150–7163.
43. Weide K, Kuhl K, Schinke R. Unstable periodic orbits, recurrences, and diffuse vibrational structures in the photodissociation of water near 128 nm. *J Chem Phys* 1989, 91:3999–4008.
44. Von Dirke M, Heumann B, Schinke R, Sension RJ, Hudson BS. Emission spectroscopy of H_2O dissociating in the B^1A_1 state: rapid bending motion manifested through excitation of high bending states of H_2O (X). *J Chem Phys* 1993, 99:1050–1056.
45. Von Dirke M, Heumann B, Kuhl K, Schroder T, Schinke R. Fluctuations in absorption spectra and final product state distributions following photodissociation processes. *J Chem Phys* 1994, 101: 2051–2068.
46. van Harrevelt R, van Hemert MC. Photodissociation of water. II. Wave packet calculations for the photofragmentation of H_2O and D_2O in the B band. *J Chem Phys* 2000, 112:5787–5808.
47. Jiang B, Xie DQ, Guo H. State-to-state photodissociation dynamics of triatomic molecules: H_2O in the B band. *J Chem Phys* 2012, 136:034302.
48. Flouquet F, Horsley JA. *Ab initio* study of potential energy surface of B^1A_1 excited state of H_2O. *J Chem Phys* 1974, 60:3767–3772.
49. Theodorakopoulos G, Petsalakis ID, Buenker RJ. MRD CI calculations on the asymmetric stretch potentials of H_2O in the ground and the first seven singlet excited states. *Chem Phys* 1985, 96:217–225.
50. Segev E, Shapiro M. Three-dimensional quantum dynamics of H_2O and HOD photodissociation. *J Chem Phys* 1982, 77:5604–5623.
51. Dixon RN. The role of inter-state Renner-Teller coupling in the dissociation of triatomic molecules. A time-dependent approach. *Mol Phys* 1985, 54:333–350.
52. Dunne LJ, Guo H, Murrell JN. The role of the B–X conical intersection in the photodissociation of water. *Mol Phys* 1987, 62:283–294.
53. Weide K, Schinke R. Photodissociation dynamics of water in the second absorption band. I. Rotational state distributions of OH($^2\Sigma$) and OH($^2\Pi$). *J Chem Phys* 1987, 87:4627–4633.
54. Guo H. The B state photodissociation of water: a classical trajectory study. *Mol Phys* 1989, 68:249–254.
55. Heumann B, Kuhl K, Weide K, Duren R, Hess B, Meier U, Peyerimhoff SD, Schinke R. Photodissociation dynamics of water in the second absorption band: vibrational excitation of OH($\tilde{A}^2\Sigma$). *Chem Phys Lett* 1990, 166:385–390.
56. Dixon RN. Λ-doublet and spin-doublet population distributions in the products of photofragmentation via coupled electronic channels: $H_2O(B^1A_1) \rightarrow H + OH(X^2\Pi)$. *J Chem Phys* 1995, 102:301–309.
57. Yarkony DR. On the description of potential energy surfaces exhibiting conical intersections: a compact representation of the energies and derivative couplings and locally diabatic bases for the HOH and OHH portions of the $1^1A'$–$2^1A'$ seam of conical intersection in water. *Mol Phys* 1998, 93:971–983.
58. van Harrevelt R, van Hemert MC. Photodissociation of water. I. Electronic structure calculations for the excited states. *J Chem Phys* 2000, 112:5777–5786.
59. van Harrevelt R, van Hemert MC, Schatz GC. A comparative classical-quantum study of the photodissociation of water in the B band. *J Phys Chem A* 2001, 105:11480–11487.
60. van Harrevelt R, van Hemert MC. Quantum mechanical calculations for the $H_2O + h\nu \rightarrow O(^1D) + H_2$ photodissociation process. *J Phys Chem A* 2008, 112:3002–3009.
61. Carrington T. Angular momentum distribution and emission spectrum of OH($^2\Sigma^+$) in photodissociation of H_2O. *J Chem Phys* 1964, 41:2012–2018.
62. Hodgson A, Simons JP, Ashfold MNR, Bayley JM, Dixon RN. Quantum state-selected photodissociation dynamics in H_2O and D_2O. *Mol Phys* 1985, 54:351–368.

63. Krautwald HJ, Schnieder L, Welge KH, Ashfold MNR. Hydrogen-atom photofragment spectroscopy. Photodissociation dynamics of H_2O in the *B–X* absorption band. *Faraday Discuss* 1986, 82:99–110.
64. Mordaunt DH, Ashfold MNR, Dixon RN. Dissociation dynamics of $H_2O(D_2O)$ following photoexcitation at the Lyman-α wavelength (121.6 nm). *J Chem Phys* 1994, 100:7360–7375.
65. Dixon RN, Hwang DW, Yang XF, Harich S, Lin JJ, Yang X. Chemical "double slits": dynamical interference of photodissociation pathways in water. *Science* 1999, 285:1249–1253.
66. Hwang DW, Yang XF, Harich S, Lin JJ, Yang X. Photodissociation dynamics of H_2O at 121.6 nm: effect of parent rotational excitation on reaction pathways. *J Chem Phys* 1999, 110:4123–4126.
67. Zanganeh AH, Fillion JH, Ruiz J, Castillejo M, Lemaire JL, Shafizadeh N, Rostas F. Photodissociation of H_2O and D_2O below 132 nm. *J Chem Phys* 2000, 112:5660–5671.
68. Harich SA, Hwang DWH, Yang XF, Lin JJ, Yang XM, Dixon RN. Photodissociation of H_2O at 121.6 nm: a state-to-state dynamical picture. *J Chem Phys* 2000, 113:10073–10090.
69. Harich SA, Yang XF, Hwang DWH, Lin JJ, Yang XM, Dixon RN. Photodissociation of D_2O at 121.6 nm: a state-to-state dynamical picture. *J Chem Phys* 2001, 114:7830–7837.
70. Harich SA, Yang YF, Yang XM. Extremely rotationally excited OH from water (HOD) photodissociation through conical intersection. *Phys Rev Lett* 2001, 87:253201.
71. Fillion JH, van Harrevelt R, Ruiz J, Castillejo N, Zanganeh AH, Lemaire JL, van Hemert MC, Rostas F. Photodissociation of H_2O and D_2O in *B*, *C*, and *D* states (134–119 nm). Comparison between experiment and *ab initio* calculations. *J Phys Chem A* 2001, 105:11414–11424.
72. Underwood J, Wittig C. Two-photon photodissociation of H_2O via the *B* state. *Chem Phys Lett* 2004, 386:190–195.
73. Cheng BM, Chung CY, Bahou M, Lee YP, Lee LC, van Harrevelt R, van Hemert MC. Quantitative spectroscopic and theoretical study of the optical absorption spectra of H_2O, HOD, and D_2O in the 125–145 nm region. *J Chem Phys* 2004, 120:224–229.
74. Cheng Y, Yuan K, Cheng L, Guo Q, Dai D, Yang X. Photodissociation dynamics of H_2O: effect of unstable resonances on the B^1A_1 electronic state. *J Chem Phys* 2011, 134:064301.
75. Zhou L, Jiang B, Xie D, Guo H. State-to-state photodissociation dynamics of H_2O in the *B* band: competition between two coexisting nonadiabatic pathways. *J Phys Chem A* 2013, 117:6940–6947.
76. Wang HT, Felps WS, McGlynn SP. Molecular Rydberg states. VII. Water. *J Chem Phys* 1977, 67:2614–2628.
77. Kuge HH, Kleinermanns K. Rotational predissociation of H_2O (C^1B_1) studied by multiphoton ionization spectroscopy in a supersonic free jet. *J Chem Phys* 1989, 90:46–52.
78. Ashfold MNR, Bayley JM, Dixon RN. The $4s \leftarrow 1b_1$ and $3d \leftarrow 1b_1$ Rydberg states of H_2O and D_2O: spectroscopy and predissociation dynamics. *Can J Phys* 1984, 62:1806–1833.
79. Ashfold MNR, Bayley JM, Dixon RN. Molecular predissociation dynamics revealed through multiphoton ionisation spectroscopy. I. The C^1B_1 states of H_2O and D_2O. *Chem Phys* 1984, 84:35–50.
80. Yang CH, Sarma G, ter Meulen JJ, Parker DH, Western CM. REMPI spectroscopy and predissociation of the $C^1B_1(\nu = 0)$ rotational levels of H_2O, HOD and D_2O. *Phys Chem Chem Phys* 2010, 12:13983–13991.
81. Yuan K, Cheng Y, Cheng L, Guo Q, Dai D, Wang X, Yang X, Dixon RN. Nonadiabatic dissociation dynamics in H_2O: competition between rotationally and nonrotationally mediated pathways. *Proc Natl Acad Sci U S A* 2008, 105:19148–19153.
82. Meijer G, Termeulen JJ, Andresen P, Bath A. Sensitive quantum state selective detection of H_2O and D_2O by (2 + 1)-resonance enhanced multiphoton ionization. *J Chem Phys* 1986, 85:6914–6922.
83. Fotakis C, McKendrick CB, Donovan RJ. Two-photon excitation of H_2O and D_2O with a KrF laser (248 nm): photofragment fluorescence from OH and OD($A^2\Sigma^+$). *Chem Phys Lett* 1981, 80:598–600.
84. Yuan K, Cheng Y, Cheng L, Guo Q, Dai D, Yang X, Dixon RN. Quantum state-selected photodissociation dynamics of H_2O: two-photon dissociation via the *C* electronic state. *J Chem Phys* 2010, 133:134301.
85. Cheng Y, Cheng L, Guo Q, Yuan K, Dai D, Wang X, Dixon RN, Yang X. Rotational state specific dissociation dynamics of D_2O via the *C* electronic state. *J Chem Phys* 2010, 133:034307.
86. Cheng L, Yuan K, Cheng Y, Guo Q, Wang T, Dai D, Yang X, Dixon RN. Rotational state specific dissociation dynamics of HOD → H + OD via two-photon excitation to the *C* electronic state. *J Phys Chem A* 2011, 115:1500–1507.
87. Cheng L, Yuan K, Cheng Y, Guo Q, Yang X, Dixon RN. Product rotational Franck–Condon oscillations in HOD ($J_{ka,kc}$) dissociation. *Mol Phys* 2010, 108:905–914.
88. Dixon RN, Oliver TAA, Cheng L, Cheng Y, Yuan K, Yang X. Vibronically induced decay paths from the C^1B_1-state of water and its isotopomers. *J Chem Phys* 2013, 138:104306.

89. Hirst DM, Child MS. *Ab initio* bending potential energy curves for Rydberg states of H_2O. *Mol Phys* 1992, 77:463–476.
90. Steinkellner O, Noack F, Ritze HH, Radloff W, Hertel IV. Ultrafast predissociation dynamics of water molecules excited to the electronic *C* and *D* states. *J Chem Phys* 2004, 121:1765–1770.
91. Langhoff SR, Davidson ER. Configuration interaction calculations on nitrogen molecule. *Int J Quantum Chem* 1974, 8:61–72.
92. Knowles PJ, Werner HJ. An efficient method for the evaluation of coupling coefficients in configuration interaction calculations. *Chem Phys Lett* 1988, 145:514–522.
93. Werner HJ, Knowles PJ. An efficient internally contracted multiconfiguration–reference configuration interaction method. *J Chem Phys* 1988, 89:5803–5814.
94. Dobbyn AJ, Knowles PJ. A comparative study of methods for describing non-adiabatic coupling: diabatic representation of the $^1\Sigma^+/^1\Pi$ HOH and HHO conical intersections. *Mol Phys* 1997, 91:1107–1123.
95. Jiang B, Xie DQ, Guo H. Communication: state-to-state differential cross sections for $H_2O(B)$ photodissociation. *J Chem Phys* 2011, 134:231103.
96. Kendall RA, Dunning TH, Harrison RJ. Electron affinities of the first-row atoms revisited. Systematic basis sets and wave functions. *J Chem Phys* 1992, 96:6796–6806.
97. Werner H-J, Knowles PJ, Lindh R, Manby FR, Schütz M, Celani P, Korona T, Rauhut G, Amos RD, Bernhardsson A, et al. MOLPRO, version 2006.1, a package of *ab initio* programs. 2006. Available at: http://www.molpro.net. (Accessed November 14, 2015).
98. Werner HJ, Follmeg B, Alexander MH. Adiabatic and diabatic potential energy surfaces for collisions of $CN(X^2\Sigma^+,A^2\Pi)$ with He. *J Chem Phys* 1988, 89:3139–3151.
99. Simah D, Hartke B, Werner HJ. Photodissociation dynamics of H_2S on new coupled *ab initio* potential energy surfaces. *J Chem Phys* 1999, 111:4523–4534.
100. Zhang JZH. *Theory and Application of Quantum Molecular Dynamics*. Singapore: World Scientific; 1999.
101. Goldfield EM, Gray SK, Harding LB. Quantum dynamics of Renner–Teller vibronic coupling: the predissociation of HCO. *J Chem Phys* 1993, 99:5812–5827.
102. Carter S, Handy NC. A variational method for the calculation of ro-vibronic levels of any orbitally degenerate (Renner–Teller) triatomic molecule. *Mol Phys* 1984, 52:1367–1391.
103. Tennyson J, Sutcliffe BT. Variationally exact ro-vibrational levels of the floppy CH^{2+} molecule. *J Mol Spectrosc* 1983, 101:71–82.
104. Petrongolo C. Nonadiabatic theory of triatomics: general formalism and application to Renner–Teller and conical-intersection effects. *J Chem Phys* 1988, 89:1297–1308.
105. Zhou LS, Xie DQ, Guo H. Signatures of non-adiabatic dynamics in the fine-structure state distributions of the OH(*X*/*A*) products in the *B* band photodissociation of H_2O. *J Chem Phys* 2015, 142:124317.
106. Brown JM, Hougen JT, Huber KP, Johns JWC, Kopp I, Lefebvrebrion H, Merer AJ, Ramsay DA, Rostas J, Zare RN. Labeling of parity doublet levels in linear molecules. *J Mol Spectrosc* 1975, 55: 500–503.
107. Hougen JT. Rotational structure of singlet–triplet transitions in near symmetric tops. *Can J Phys* 1964, 42:433–451.
108. Mandelshtam VA, Taylor HS. A simple recursion polynomial expansion of the Green's function with absorbing boundary conditions. Application to the reactive scattering. *J Chem Phys* 1995, 103:2903–2907.
109. Chen RQ, Guo H. Evolution of quantum system in order domain of Chebyshev operator. *J Chem Phys* 1996, 105:3569–3578.
110. Guo H. A time-independent theory of photodissociation based on polynomial propagation. *J Chem Phys* 1998, 108:2466–2472.
111. Balint-Kurti GG. Wavepacket theory of photodissociation and reactive scattering. In: Rice RA, ed. *Advances in Chemical Physics*, vol. 128. Hoboken, NJ: John Wiley & Sons; 2004, 249–301.
112. Balint-Kurti GG, Shapiro M. Photofragmentation of triatomic molecules. Theory of angular and state distribution of product fragments. *Chem Phys* 1981, 61:137–155.
113. Balint-Kurti GG, Dixon RN, Marston CC. Time-dependent quantum dynamics of molecular photofragmentation processes. *J Chem Soc Faraday Trans* 1990, 86:1741–1749.
114. Balint-Kurti GG. Wavepacket quantum dynamics. *Theor Chem Acc* 2010, 127:1–17.
115. Xie DQ, Guo H, Amatatsu Y, Kosloff R. Three-dimensional photodissociation dynamics of rotational state selected methyl iodide. *J Phys Chem A* 2000, 104:1009–1019.
116. Guo H, Seideman T. Quantum mechanical study of photodissociation of oriented $ClNO(S_1)$. *Phys Chem Chem Phys* 1999, 1:1265–1272.
117. DG X, Xie DQ, Guo H. Theoretical study of predissociation dynamics of HCN/DCN in their first absorption bands. *J Chem Phys* 2002, 116:10626–10635.
118. Heumann B, Weide K, Duren R, Schinke R. Nonadiabatic effects in the photodissociation of H_2S in the

first absorption band: an *ab initio* study. *J Chem Phys* 1993, 98:5508–5525.

119. Vanderwal RL, Scott JL, Crim FF. State resolved photodissociation of vibrationally excited water: rotations, stretching vibrations, and relative cross sections. *J Chem Phys* 1991, 94:1859–1867.
120. Plusquellic DF, Votava O, Nesbitt DJ. Bond-selective photofragmentation of jet-cooled HOD at 193 nm: vibrationally mediated photochemistry with zero-point excitation. *J Chem Phys* 1998, 109:6631–6640.
121. Votava O, Plusquellic DF, Nesbitt DJ. Vibrationally mediated photolysis dynamics of H_2O in the υ(OH) = 3 manifold: far off resonance photodissociation cross sections and OH product state distributions. *J Chem Phys* 1999, 110:8564–8576.
122. Nizkorodov SA, Ziemkiewicz M, Myers TL, Nesbitt DJ. Vibrationally mediated dissociation dynamics of H_2O in the ν(OH) = 2 polyad. *J Chem Phys* 2003, 119:10158–10168.
123. Rosenwaks S. *Vibrationally Mediated Photodissociation*. Cambridge: Royal Society of Chemistry; 2009.
124. Staemmler V, Palma A. CEPA calculations of potential energy surfaces for open-shell systems. IV. Photodissciation of H_2O in the A^1B_1 state. *Chem Phys* 1985, 93:63–69.
125. Hwang DW, Yang XF, Yang XM. The vibrational distribution of the OH product from H_2O photodissociation at 157 nm: discrepancies between theory and experiment. *J Chem Phys* 1999, 110:4119–4122.
126. van Harrevelt R, van Hemert MC. Photodissociation of water in the *A* band revisited with new potential energy surfaces. *J Chem Phys* 2001, 114:9453–9462.
127. Yang XF, Hwang DW, Lin JJ, Ying X. Dissociation dynamics of the water molecule on the $\tilde{A}^1B_1$ electronic surface. *J Chem Phys* 2000, 113:10597–10604.
128. Cheng BM, Chew EP, Liu CP, Bahou M, Lee YP, Yung YL, Gerstell MF. Photo-induced fractionation of water isotopomers in the Martian atmosphere. *Geophys Res Lett* 1999, 26:3657–3660.
129. Lu IC, Wang F, Yuan K, Cheng Y, Yang X. Nonstatistical spin dynamics in photodissociation of H_2O at 157 nm. *J Chem Phys* 2008, 128:066101.
130. van Harrevelt R, van Hemert MC. Photodissociation of warm water: *ab initio* calculations of the room-temperature absorption spectrum. *Chem Phys Lett* 2003, 370:706–711.
131. Harich SA, Yang XF, Yang X, van Harrevelt R, van Hemert MC. Single rotational product propensity in the photodissociation of HOD. *Phys Rev Lett* 2001, 87:263001.
132. Zhou LS, Lin GSM, Xie DQ. State to state photodissociation dynamics of D_2O in the *B* band. *J Chem Phys* 2013, 139:114303.
133. Han SY, Zhou LS, Xie DQ. State to state photodissociation dynamics of vibrationally excited D_2O in *B* band. *Chin J Chem Phys* 2015, 28:396–402.
134. Cheng Y, Cheng L, Guo Q, Yuan K, Dai D, Yang X. Photodissociation dynamics of D_2O via the B^1A_1 electronic state. *J Chem Phys* 2011, 134:104305.
135. Crim FF. Bond-selected chemistry: vibrational state control of photodissociation and bimolecular reaction. *J Phys Chem* 1996, 100:12725–12734.
136. Engel V, Schinke R. Isotope effects in the fragmentation of water: the photodissociation of HOD in the first absorption band. *J Chem Phys* 1988, 88:6831–6837.
137. Zhang JZ, Imre DG. OH/OD bond breaking selectivity in HOD photodissociation. *Chem Phys Lett* 1988, 149:233–238.
138. Zhang JZ, Imre DG, Frederick JH. HOD spectroscopy and photodissociation dynamics: selectivity in OH/OD bond breaking. *J Phys Chem* 1989, 93:1840–1851.
139. Imre DG, Zhang JH. Dynamics and selective bond breaking in photodissociation. *Chem Phys* 1989, 139:89–121.
140. Hartke B, Manz J, Mathis J. Mode selective control of unimolecular dissociations: survey, and model simulations for HDO → H + DO, D + HO. *Chem Phys* 1989, 139:123–146.
141. Vanderwal RL, Scott JL, Crim FF. Selectively breaking the OH bond in HOD. *J Chem Phys* 1990, 92:803–805.
142. Bar I, Cohen Y, David D, Rosenwaks S, Valentini JJ. Direct observation of preferential bond fission by excitation of a vibrational fundamental: photodissociation of HOD (0, 0, 1). *J Chem Phys* 1990, 93:2146–2148.
143. Bar I, Cohen Y, David D, Arusiparpar T, Rosenwaks S, Valentini JJ. Mode-selective bond fission: comparison between the photodissociation of HOD (0, 0, 1) and HOD (1, 0, 0). *J Chem Phys* 1991, 95:3341–3346.
144. Vanderwal RL, Scott JL, Crim FF, Weide K, Schinke R. An experimental and theoretical study of the bond selected photodissociation of HOD. *J Chem Phys* 1991, 94:3548–3555.
145. Akagi H, Fukazawa H, Yokoyama K, Yokoyama A. Selective OD bond dissociation of HOD: photodissociation of vibrationally excited HOD in the $5\nu_{OD}$ state. *J Chem Phys* 2005, 123:184305.
146. Su S, Wang H, Chen Z, Yu S, Dai D, Yuan K, Yang X. Photodissociation dynamics of HOD via the $B(^1A_1)$ electronic state. *J Chem Phys* 2015, 143:184302.
147. Zhou LS, Xie DQ. Full-dimensional quantum dynamics of vibrational mediated photodissociation of HOD in its *B* band. *J Phys Chem A* 2015, 119:12062–12072.

